NJC

Facile synthesis of mesoporous TiO2 film templated by block copolymer for photocatalytic applications

Journal:	*New Journal of Chemistry*
Manuscript ID	NJ-ART-06-2021-002997.R1
Article Type:	Paper
Date Submitted by the Author:	13-Jul-2021
Complete List of Authors:	Olatidoye, Olufemi; North Carolina Agricultural and Technical State University College of Arts and Sciences, Chemistry Thomas, Daria; North Carolina Agricultural and Technical State University College of Arts and Sciences, Chemistry Bastakoti, Bishnu; North Carolina Agricultural and Technical State University College of Arts and Sciences, Chemistry

Facile synthesis of mesoporous TiO_2 film templated by block copolymer for photocatalytic applications

Olufemi Olatidoye, Daria Thomas and Bishnu P. Bastakoti*

Department of Chemistry

North Carolina A&T State University

bpbastakoti@ncat.edu

A facile synthesis of a mesoporous TiO_2 thin film is reported using poly(styrene-2-vinyl pyridine-ethylene oxide) polymeric micelle as a synthetic template. As the Ti precursor strongly binds with polymeric micelles in solution (before evaporation), the controlled condition such as temperature and relative humidity is not required for self-assembly of molecularly dissolved polymer and Ti sources. The mesoporous TiO_2 films have enhanced photocatalytic activity due to increased surface area and rough surface around the pores. Photocatalytic testing with methylene blue dye showed that the prepared mesoporous thin films were effective in degrading dye. Degradation of methylene blue dye with nonporous TiO_2 yielded a shift in the max absorption wavelength that is proposed to be the result of dimerization of methylene blue molecules during photocatalytic degradation.

Introduction

As environmental pollution continues to worsen, technologies and materials that mitigate these issues have become a widely researched topic.[1] In particular, technologies that employ photochemistry have become especially attractive due to the abundance of solar energy that is available for use. The principle behind photocatalysis is the generation of holes in valence bands through the excitation of electrons by photons. The holes created by photoexcitation serve as redox sources where radical species are produced and decomposition reactions can take place.[2] Semiconductor photocatalysts (TiO_2, ZnO, Fe_2O_3, WO_3, CuS, and more) have a wide range of applications including use in water and air purification, fuel production, energy production, and gas sensing.[3-6]

Titania (TiO_2) is one of the most widely studied semiconductor photocatalysts with great potential due to its strong redox ability under UV irradiation, nontoxicity, high stability, low price, and high photocatalytic efficiency.[7,8] Photodegradation with TiO_2 proceeds through a photoexcitation mechanism that produces reactive radical species that can decompose chemical compounds.[9] Since TiO_2 is a semiconductor, its valence band is full of electrons and its conduction band is empty. Semiconducting materials have a bandgap that is favorable for the generation of valence band holes during photoexcitation. The holes occur when a photon with a certain amount of energy ($\geq$ bandgap) is absorbed. This causes an electron in the valence band to get excited and move to the conduction band, leaving behind a hole in the valence band. The excited electrons and the valence band holes can be used for oxidizing oxygen and water molecules. The produced hydroxyl radicals can oxidize pollutant molecules adsorbed on the semiconductor surface.

TiO_2 photocatalysts can be prepared with a variety of nanostructures. Electrospinning,[10] sol-gel,[11] and hydrothermal methods[12] are commonly used for TiO_2 photocatalyst synthesis. These

methods can yield TiO_2 nanofibers, mesoporous/nonporous films, and micro/macroporous arrays. Mesoporous TiO_2 materials have become increasingly attractive for photocatalysis due to their increased surface area and easily accessible pores.[13] It has been shown that photocatalytic activity depends heavily on the surface area of the photocatalytic material. Therefore, the increased surface area allows for more photocatalytic reactions to take place and better photocatalytic activity is observed. Sol-gel methods are favorable for the synthesis of porous TiO_2 because they can be done without the use of complex equipment and can be done under ambient pressure and temperature.[14] Sol-gel synthesis of porous TiO_2 typically involves a hydrolysis-condensation of a metal source (titanium alkoxides such as titanium butoxide/tetraisopropoxide) to form an oxo-hydroxide that subsequently becomes the intended metal oxide; TiO_2. Sol-gel synthetic methods are highly customizable through pH and temperature control. This allows for tuning of porous TiO_2 properties such as pore size and wall thickness.[15] Sol-gel methods using different types of soft templates (polymer, surfactant, air bubble, water droplets) are widely used to synthesize porous nanostructure.[16] The pluronics family of polymer (F127, P123, and P108) leads to the formation of large-sized mesopores (around 10 nm) compared to the pores prepared with low molecular weight surfactants (CTAB, SDS).[17-21] It is still challenging to control the porosity and the porous structure collapsed at higher temperatures due to the lower thermal degradation temperature of the template used.[22]

Herein, we present a facile one-pot synthesis method for a large-sized mesoporous TiO_2 thin film using triblock copolymer micelles as a template. A triblock copolymer with chemically rich and distinct blocks was used as a stabilizer and template. The robust micelles with a rigid core and reactive shell stabilized the polymer-inorganic nanoaggregates even after loading inorganic sources. The micelles assembly along with inorganic source followed by calcination gives a

mesoporous structure with 35-45 nm pore size. The porous film was tested as a photocatalyst to degrade organic dyes; methylene blue (MB). The comparison study of degradation on nonporous film found that the dyes degraded faster in mesoporous film. Dimerization of MB was observed before degradation in nonporous film.

Experimental

Materials

Poly(styrene-*b*-2-vinyl pyridine-*b*-ethylene oxide) triblock copolymer ($PS_{(13,000)}$-$PVP_{(9,000)}$-$EO_{(16,500)}$, Polymer Source, Inc.) was used as the template. Titanium tetraisopropoxide (TTIP; Fisher Chemical), tetrahydrofuran (THF; Fisher Chemical), hydrochloric acid (HCl; Fisher Chemical), and methylene blue organic dye (MB; Alfa Aesar) were used without any further purification.

TiO_2 thin film synthesis

PS-PVP-PEO micelles were used as a template for the synthesis of mesoporous TiO_2 thin films. 20 mg PS-PVP-PEO triblock copolymer was dissolved in 4 mL of THF at room temperature using mild sonication for 20 min. To produce micellization of the polymer, hydrochloric acid (80 μL) was added into the solution and the mixture was stirred magnetically for 30 minutes. TTIP (80 μL) was added and the solution was stirred for another 30 minutes. After stirring, the solution (400 μL) was spread across glass slides to create thin films or allowed to evaporate in a petri dish. The films were allowed to dry at room temperature for 24 hours followed by calcination at 550 ºC in the air at a ramping rate of 2 ºC/min. Nonporous TiO_2 films were also synthesized without PS-PVP-PEO triblock copolymer micelles.

Characterization

Hydrodynamic diameter and zeta potential of polymeric micelles were measured using Otsuka ELS Z zeta-potential and particle analyzer. All the measurements were carried out at 25 °C. The correlation functions were analyzed by the contin method and used to determine the diffusion coefficient (D) of the particles. The hydrodynamic diameter (D_h) was calculated from D using the Stokes-Einstein equation ($D_h=K_BT/3\pi\eta D$). Here K_B is the Boltzmann constant, T is the absolute temperature and η is the solvent viscosity. The morphology of polymeric micelles and porous TiO_2 were observed under field emission scanning electron microscopy (SEM; Hitachi SU-8000) and transmission electron microscopy (TEM; JEOL JEM-1210). The crystalline phases and crystallinity were measured by X-ray powder diffraction (XRD; Shimadzu XRD-7000) analysis. Raman spectra were measured using a Raman spectrometer (T64000: Jobin-Yvon). The removal of the polymer was confirmed by thermal gravimetric analysis (Seiko-6300 TG/DTA) and Fourier Transform infrared spectroscopy (Shimadzu: FTIR equipped with an MCT detector). The surface area was determined by a Quantachrom surface area analyzer.

Photocatalytic testing

The decomposition of MB organic dye was observed under UV irradiation over time to study the photocatalytic efficiency of the mesoporous TiO_2 thin film. UV irradiation was facilitated by a UV lamp. The TiO_2 on the glass slide was submerged in an MB solution (3 ppm, 10 mL) and left in the dark at room temperature for 30 minutes for equilibration. The submerged film was put under UV irradiation with the lamp and the decomposition of the MB dye was observed by measuring the absorbance at 30-minute intervals with a UV-Visible spectrophotometer. The degradation of MB and MB dimer was monitored by analyzing absorbance at 666 nm and 604 nm respectively. The used film was washed with water and dried at 65 ^oC in a vacuum for 1h to reuse.

Results and Discussion

The molecularly dissolved polymer in THF undergoes self-assembly after the addition of hydrochloric acid solution. The clear polymer solution turns turbid (milky) confirming the formation of the micelles (**Figure 1b**). 85 nm micelles with a positive surface charge (28 mV) are realized using a dynamic light scattering experiment at room temperature. **Figure 1d** tabulated the hydrodynamic diameters of polymer in different solutions. The spherical micelles are observed under high emission scanning electron microscope (**Figure 2a**). The self-assembly of polymeric micelles occurs due to an increase in the interfacial energy between hydrophobic polystyrene and polar hydrochloric acid. The polar nature of HCl makes it a poor solvent for the hydrophobic PS block of PS-PVP-PEO block copolymer. Spherical micelles with PS core, PVP shell, and PEO corona are expected in THF/HCl solution.[23] The positive charge on the micelles comes from the PVP block, as it is protonated in acidic conditions. The pH of the solution is maintained below the pK_a (4.5) value of PVP.[24] The good balance among hydrophobic PS, positively charged hydrophilic PVP and hydrophilic PEO makes the polymeric micelles stable for a prolonged time. PVP is a reaction site for inorganic precursors. Inorganic precursors are believed to interact with PVP via electrostatic or co-ordinate covalent or H-bonding.[25] Titanium tetraisopropoxide (TTIP) was used as the TiO_2 source into the polymer solution. After the addition of TTIP, the size of the micelles decreases to 65 nm. The change in size is attributed to the strong binding of TTIP to the polymeric micelles.

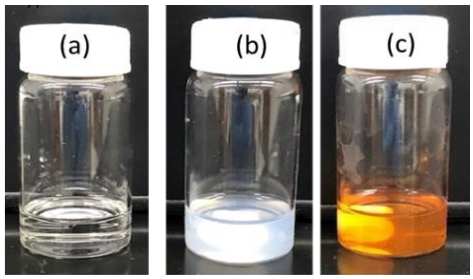

(d)

Sample	D_h/nm
Polymer in THF	0
Polymer in THF/HCl	85
Polymer in THF/HCl/TTIP	65

Figure 1. Photos of polymer solution in (a) THF, (b) THF/HCl and (c) THF/HCl/TTIP. (d) the hydrodynamic diameter of polymer solutions are shown.

Almost 0 mV zeta potential indicates that the TTIP masks the positive charge of PVP. The confined hydrolysis and condensation reaction of TTIP takes place around the rigid polystyrene core. The strong interaction of polymeric micelles with the inorganic source makes the method versatile. The polymer nanoaggregates are stable even after loading the inorganic source. The polymer composites were casted on glass slides or left for solvent evaporation in a petri dish. The evaporation of solvents induces micelles assembly to form polymer composites compact structure.

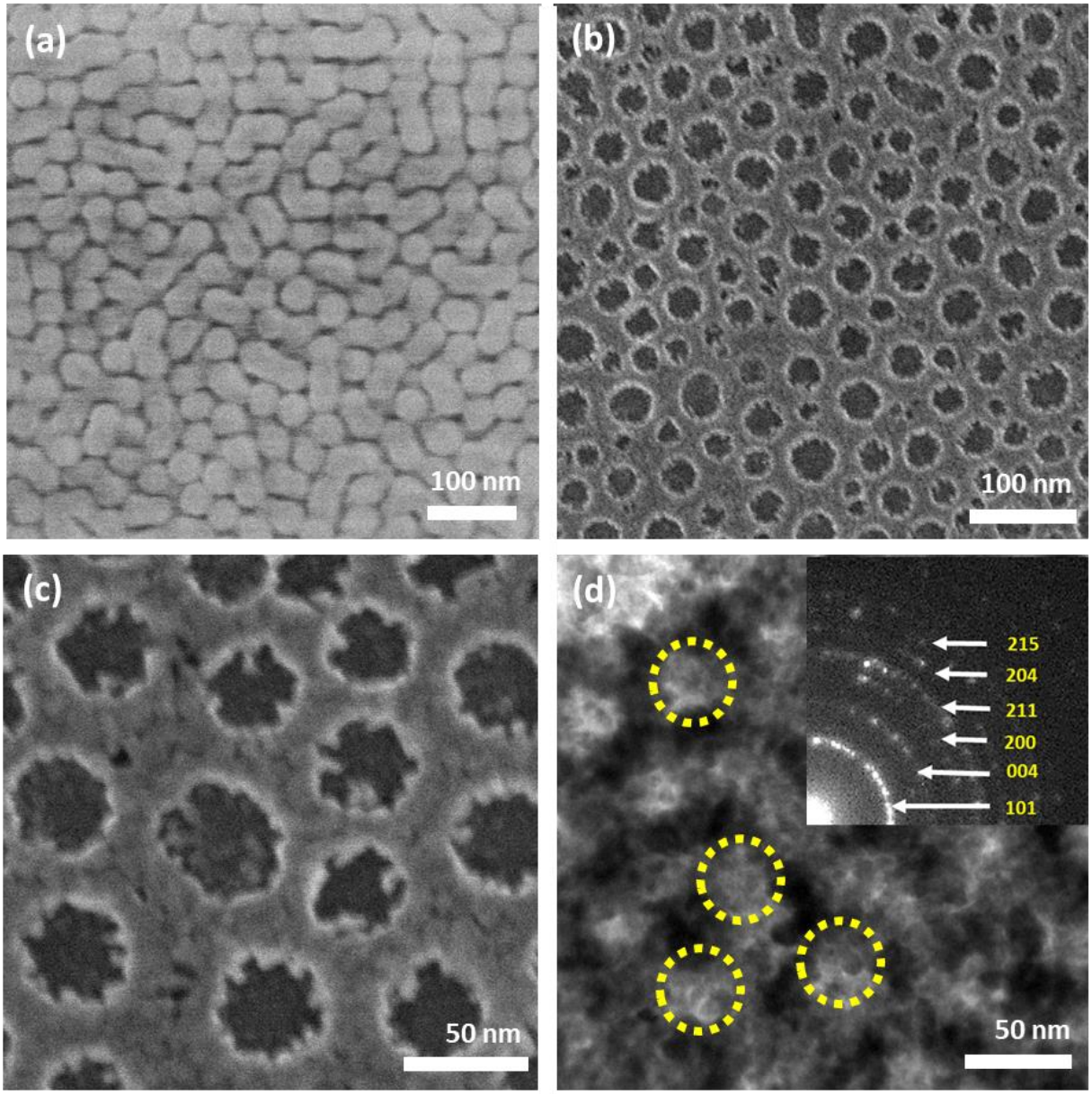

Figure 2. SEM images of (a) polymeric micelles, (b,c) mesoporous TiO_2. (d) TEM images of mesoporous TiO_2. The yellow circle highlights the mesopores. Selected electron diffraction pattern is shown in inset.

As the Ti precursors strongly bind with polymer in solution (before evaporation), the controlled conditions such as temperature and relative humidity are not required for self-assembly of molecularly dissolved polymer and metal sources as realized in conventional evaporation induced self-assembly. The polymer composites were calcined at 550 ^{o}C to remove the polymeric template. The calcination burns out the polymer leaving a porous crystalline framework of TiO_2. **Figure 2b-c** shows the SEM images of the mesoporous framework of TiO_2. The high-resolution SEM image clearly shows the pore size at the range of 35-45 nm with a thick wall of TiO_2. The opening of pores has lots of rough surfaces that provide space for incoming molecules during catalysis. By varying the molecular weight and solvent compositions, the pore size could be controlled in nanoscale.[26] The yellow circles represent the mesopores in TEM images. The BET isotherm (**Figure S1**) was of type IV, representing the mesoporous TiO_2 with a surface area of 90.3 $m^2.g^{-1}$.

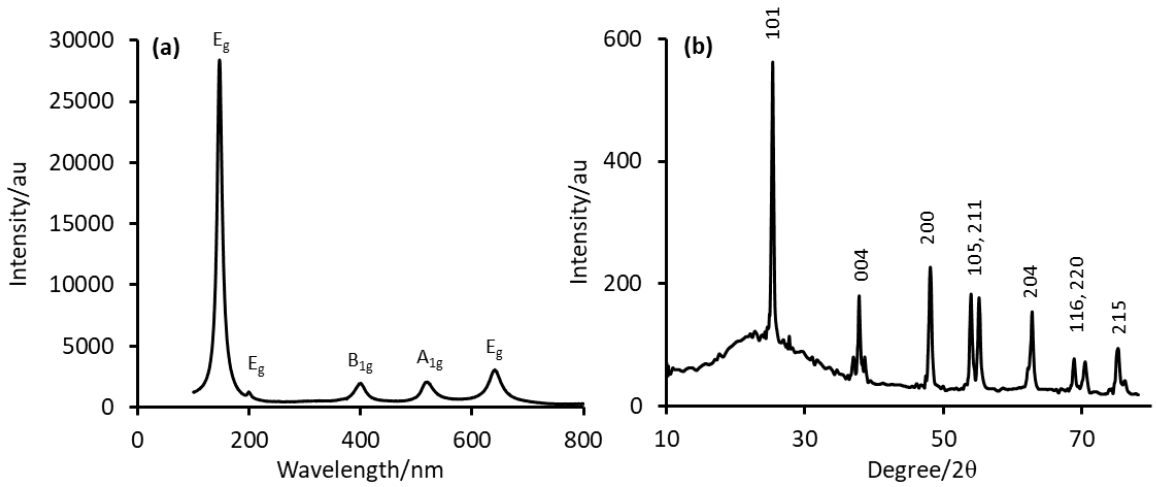

Figure 3. Raman and XRD spectra of mesoporous TiO_2.

Among the three polymorphs of TiO_2 (anatase, brookite, and rutile), anatase is considered the best photocatalyst having the lowest crystallization temperature.[27] The anatase form transforms to rutile at higher temperatures.[28] We obtained the anatase phase of TiO_2 up to 700 ^{o}C. However,

the porous framework was destroyed (**Figure S2**). The observed electron diffraction pattern of (101), (004), (200), (211), and (204) and (215) are assignable to anatase crystal which is also supported by XRD and Raman spectra. The crystallinity and crystalline phase of mesoporous TiO_2 was investigated by Raman and wide-angle XRD measurements (**Figure 3**). All the peaks that appeared in the XRD profile matched with TiO_2 anatase (JCPDS 00-021-1272). Five Raman active optical phonon modes are clearly observed; E_g(147cm^{-1}), E_g (197 cm^{-1}), B_{1g} (398 cm^{-1}), A_{1g} (519 cm^{-1}), and E_{1g} (641 cm^{-1}). The E_g peaks are caused by the symmetric stretching vibration of O-Ti-O, the B_{1g} peak is caused by the symmetric bending vibration of O-Ti-O, and the A_{1g} peak is caused by the antisymmetric bending vibration of O-Ti-O in TiO_2.[29] All the peaks belong to anatase form of TiO_2.

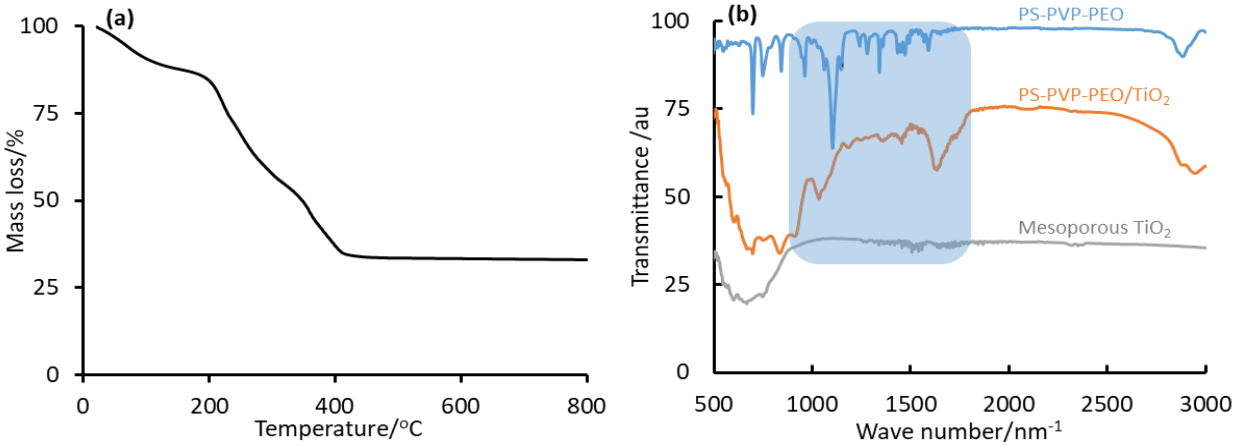

Figure 4. (a) Thermogravimetric analysis of polymer composites and (b) FTIR spectra of polymer, polymer composites, and mesoporous TiO_2.

Thermogravimetric analysis and FTIR spectra of polymer composites confirmed the removal of the polymeric template (**Figure 4**). The signature FTIR peaks of the polymer template are absent in the calcined TiO_2 sample. The large weight loss in TGA at 300-400 °C indicates the removal of polymer. The weight loss at lower temperatures indicates the evaporation of adsorbed water molecules. TGA analysis showed that the used polymeric template has higher thermal

stability than generally used soft templates (pluronics, CTAB, SDS) in sol-gel reaction to synthesize mesoporous structures.[30,31] Due to lower thermal stability, the original mesostructures are distorted and/or destroyed with an increase in calcination temperatures.[22] In our polymeric system, the mesoporous framework is completely preserved even when the calcination temperature (550 °C) is higher than the crystallization temperature (300 °C) of TiO_2. More carbon content in the polymer is beneficial to get the ordered structures of mesoporous materials. The rampant carbon content at high temperatures preserves the mesoporosity.

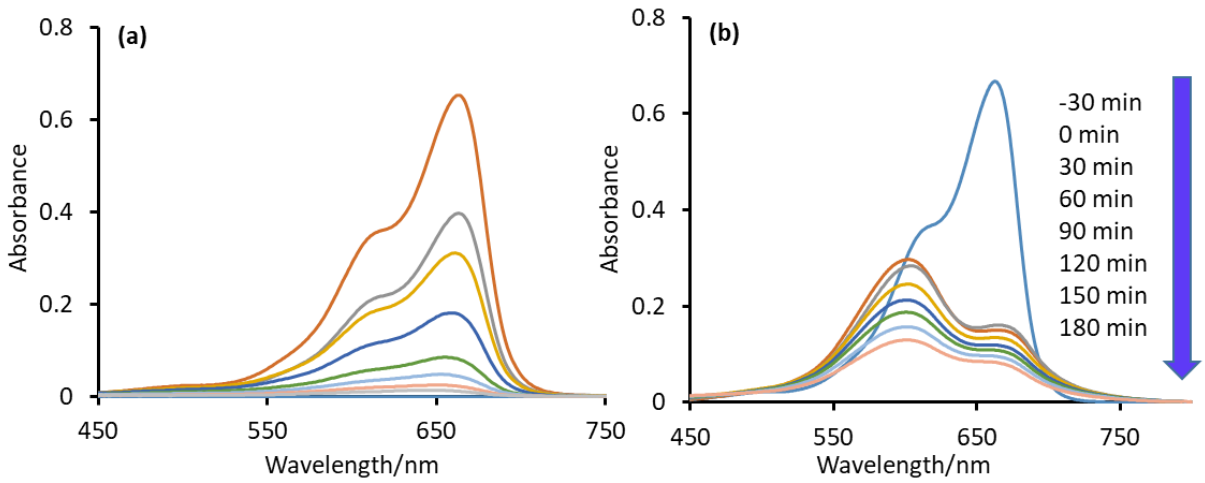

Figure 5. Absorbance spectra of MB in (a) mesoporous (b) nonporous TiO_2.

Organic dyes, one of the main by-products of the textile industry not only hurt the environment but also enter into the food chain and cause mutagenicity and carcinogenicity.[32] It has been demonstrated that TiO_2 has been widely used as a photocatalyst which is supported by the band theory of semiconductors.[33] The TiO_2 film was excited with 254 nm wavelength light to form positive holes, which further oxidize hydroxide ions (OH^-) or water to generate the hydroxyl radical ($^{\cdot}OH$). These radicals are very strong oxidants and enable to oxidize organic compounds.[34] Methylene blue was chosen as a model dye. Absorbance peak at 666 nm gradually diminished and almost disappeared after 3 hours, confirming the degradation of methylene blue under UV

irradiation. The sharp decrease in absorbance intensity during equilibration is the adsorption of dyes on/into mesoporous TiO_2. The film was easily reused after washing and found almost 100 % efficiency even after the third cycle. Nonporous TiO_2 film was used for comparison. The nonporous film was prepared without using polymeric templates. The max absorbance wavelength shifted from 666 nm to 604 nm in nonporous TiO_2 (**Figure 5b**). During equilibration, the MB molecule undergoes dimerization. The shift in max absorbance wavelength can be attributed to the dimerization of the methylene blue molecules during photocatalytic testing. MB molecules tend to aggregate in solution if the concentration of the molecules is high enough. This aggregation can yield the formation of dimers and even trimers of methylene blue molecules.[35] However, in our study dimerization was realized even at a dilute condition. This may have occurred due to the lack of pores on the film, which facilitated the aggregation of the methylene blue molecules. This dimerization likely did not occur with the mesoporous TiO_2 sample because the methylene blue molecules adhered to the pores on the thin film while undergoing the surface photocatalytic reactions. This further proves the advantages of mesoporous TiO_2 thin films. The increased surface area provided by the pores prevents the aggregation and dimerization of target molecules. The MB dimer also degrades after exposure to UV light. However, the dye degradation is much slower than in the mesoporous film.

Conclusion

In summary, mesoporous TiO_2 was successfully synthesized with the help of triblock copolymer micelle templates. The strong interaction of polymeric micelles with an inorganic source makes the method easy and versatile. The chemically rich polymeric template could be used to synthesize a wide variety of compositions. The thin films exhibited excellent photocatalytic

activity in the degradation of methylene blue dye over time. The prepared TiO_2 thin film was able to decompose MB more completely than the control sample of nonporous TiO_2 thin films under UV irradiation. MB exhibited dimerization during the testing of the nonporous thin films, proving that surface reactions for mesoporous TiO_2 differ from nonporous TiO_2. Mesoporous TiO_2 thin films have shown great potential in the realm of photocatalysis. Additionally, the dimerization of methylene blue with nonporous TiO_2 presents more avenues for future research. Photocatalysis has shown that it could provide extremely beneficial impacts to environmental protection and cleanup.

Author Information

Corresponding Author
Bishnu P. Bastakoti: Department of Chemistry, North Carolina A&T State University,
E-mail: bpbastakoti@ncat.edu

Authors

Olufemi Olatidoye: Department of Chemistry, North Carolina A&T State University
Daria Thomas: Department of Chemistry, North Carolina A&T State University

Author Contribution

Bishnu Prasad Bastakoti: Conceptualization, Investigation, Methodology, Resources, Writing - original draft, Writing - review & editing, Project administration, Funding acquisition.

Olufemi Olatidoye: Investigation, Methodology, Writing - original draft, Writing - review & editing.

Daria Thomas: Investigation and Methodology

Acknowledgment

B. P. B. thanks the National Science Foundation Research Initiation Award (2000310) USA and Joint School of Nanoscience and Nanoengineering, a member of the Southeastern Nanotechnology Infrastructure Corridor and National Nanotechnology Coordinated Infrastructure, which is supported by the National Science Foundation (Grant ECCS-1542174).

Notes

The authors declare no competing financial interest.

References

1. B. P. Bastakoti, D. Kuila, C. Salomon, M. Konarova, M. Eguchi, J. Na, Y. Yamauchi, *J Hazard. Mater.,* 2021, **401**, 123348.
2. N. Serpone, A. V. Emeline, *J. Phys. Chem. Lett.,* 2012, **3**, 673-677.
3. X. G. Yang, D. W. Wang, *ACS. Appl. Energy. Mater.,* 2018, **1**, 6657-6693.
4. Y. V. Kaneti, N.L. W. Septiani, I. Saptiama, X. Jiang, B. Yuliarto, M. J. A. Shiddiky, N. Fukumitsu, Y. Kang, D. Golberg, Y. Yamauchi, *J. Mater. Chem A*, 2019, **7**, 3415-3425.
5. J. Bentley, S. Desai, B. P. Bastakoti, *Chem. Eur. J.*, 2021, **27**, 9241-9252.
6. M. K. Bhattarai, K. K. Mishra, A. A. Instan, B.P. Bastakoti, R. S. Katiyar, *Appl. Surf. Sci.*, 2019, **490**, 451-459.
7. O. Elbanna, M. S. Zhu, M. Fujitsuka, T. Majima, *ACS Catal.,* 2019, ***9***, 3618-3626.
8. B. P. Bastakoti, Y. Sakka, K. C. W. Wu, Y. Yamauchi, *J. Nanosci. Nanotechno.* 2015, **15**, 4747-4751.
9. Q. Guo, C. Y. Zhou, Z. B. Ma, X. M. Yang, *Adv. Mater.,* 2019, **31**, 1901997.
10. C. Wang, Y. B. Tong, Z. Y. Sun, Y. Xin, E. Y. Yan, Z. H. Huang, *Mater. Lett.,* 2007, **61**, 5125-5128.
11. Y. Liang, S. J. Sun, T. R. Deng, H. Ding, W. T. Chen, Y. Chen, *Materials,* 2018, **11**, 450.
12. N. Liu, X. Y. Chen, J. L. Zhang, J. W. Schwank, *Catal Today,* 2014, **225**, 34-51.
13. W. Li, Z. X. Wu, J. X. Wang, A. A. Elzatahry, D. Y. Zhao, *Chem. Mater.* 2014, **26**, 287-298.
14. R. Sharma, A. Sarkar, R. Jha, A. K. Sharma, D. Sharma, *Int. J. Appl. Ceram. Tec.,* 2020, **17**, 1400-1409.
15. H. Choi, Y. J. Kim, R. S. Varma, D. D. Dionysiou, *Chem. Mater.,* 2006, **18**, 5377-5384.
16. B. R. Thompson, T. S. Horozov, S. D. Stoyanov, V. N. Paunov, *J. Mater. Chem. A,* 2019, **7** , 8030-8049.
17. Y. Yamauchi, K. Kuroda, *Chem-Asian J.,* 2008, **3**, 664-676.
18. A. S. Nugraha, J. Na, M. S. A. Hossaon, J. Lin, Y. V. Kaneti, M. Iqbal, B. Jiang, Y. Bando, T. Asahi, Y. Yamayuchi, *Appl. Mater. Today*, 2020, **18**, 100526.
19. F. Zhang, X. Hu, E.W. Roth, Y. Kim, S.T. Nguyen, *Chem. Mater*., 2020, **32**, 4292-4302.
20. P. Mei, Y. V. Kaneti, M. Pramanik, T. Takei, O. Dag, Y. Sugahara, Y. Yamauchi, *Nano Energy*, 2018, **52**, 336-344.
21. L. Liu, X. Yang, Y. Xie, H. Liu, X. Zhou, X. X. Xiao, Y. Ren, Z. Ma, X. Cheng, Y. Deng, D. Zhao, *Adv. Mater*., 2020, **32**, 1906653.
22. M. B. Zakaria, N. Suzuki, N. L. Torad, M. Matsuura, K. Maekawa, H. Tanabe, Y. Yamauchi, *Eur. J. Inorg. Chem.,* 2013, **13**, 2330-2335.
23. B. P. Bastakoti, Y. Li, M. Imura, N. Miyamoto, T. Nakato, T. Sasaki, Y. Yamauchi, *Angew. Chem. Int. Edit.,* 2015, **54**, 4222-4225.
24. N. Tantavichet, M. D. Pritzker, C. M. Burns, *J. Appl. Polym. Sci.,* 2001, **81**, 1493-1497.
25. B. P. Bastakoti, Y. Li, T. Kimura, Y. Yamauchi, *Small,* 2015, **11**, 1992-2002.
26. Y. Li, B. P. Bastakoti, V. Malgras, C. Li, J. Tang, J. H. Kim, Y. Yamauchi, *Angew. Chem. Int. Edit.,* 2015, **54**, 11073-11077.

27. G. Odling, N. Robertson, *Chemsuschem.,* 2015, **8**, 1838-1840.
28. N. Wetchakun, B. Incessungvorn, K. Wetchakun, S. Phanichphant, *Mater. Lett.* 2012, **82,** 195-198.
29. F. Tian, Y. P. Zhang, J. Zhang, C. X. Pan, *J. Phys. Chem. C,* 2012, **116**, 7515-7519.
30. X. Huang, W. Li, M. J. Wang, X. N. Tan, Q. Wang, C. Wang, M. N. Zhang, J. Yuan, *Sci. Rep.,* 2017, **7**, 45055.
31. D. Gu, F. Schuth, *Chem. Soc. Rev.,* 2014, **43**, 313-344.
32. A. Kongor, M. Panchal, M. Athar, M. Vora, B. Makwana, P. C. Jha, V. Jain, *Catal. Lett.,* 2021, **151**, 548-558.
33. J. Schneider, M. Matsuoka, M. Takeuchi, J. L. Zhang, Y. Horiuchi, M. Anpo, D. W. Bahnemann, *Chem. Rev.,* 2014, **114**, 9919-9986.
34. S. Gligorovski, R. Strekowski, S. Barbati, D. Vione, *Chem. Rev.,* 2015, **115**, 13051-13092.
35. A. Fernandez-Perez, G. Marban, *Acs Omega,* 2020, **5**, 29801-29815.